IEC 60270 Calibration Uncertainty in Gas-Insulated Substations

Escurra, Christian Mier; Mor, Armando Rodrigo; Vaessen, Peter

DOI
10.1109/EIC55835.2023.10177354

Publication date
2023

Document Version
Final published version

Published in
Proceedings of the 2023 IEEE Electrical Insulation Conference (EIC)

IEC 60270 Calibration Uncertainty in Gas-Insulated Substations

Christian Mier Escurra
High Voltage Technologies
Delft University of Technology
Delft, Netherlands
c.mierescurra@tudelft.nl

Armando Rodrigo Mor
Instituto de Tecnología Eléctrica
Universitat Politècnica de València
Valencia, Spain
arrodmor@ite.upv.es

Peter Vaessen
High Voltage Technologies
Delft University of Technology
Delft, Netherlands
P.T.M.Vaessen@tudelft.nl

2023 IEEE Electrical Insulation Conference (EIC) | 978-1-6654-9341-3/23/$31.00 ©2023 IEEE | DOI: 10.1109/EIC55835.2023.10177354

***Abstract*— Partial discharge (PD) measurements in gas-insulated substations (GIS) are tested according to the standard IEC 60270. This "conventional" PD test method applies to electrically small devices. The equipment size increases the resonance, and attenuation, contributing to the total uncertainty. Additionally, when an ultra-high frequency (UHF) sensor is used as a coupling capacitor, the calibrator and PD pulse duration difference increase the measurement uncertainty. In this paper, the IEC method, using an external capacitor coupler and a UHF sensor, is simulated and tested in a full-scale GIS. The results show the uncertainty dependency with the IEC 60270 filter bandwidth. With proper measures, the UHF sensor correlates with the external coupling capacitor, resulting in a reasonable charge estimation for a 25-meter-long GIS. Knowing the calibration limits is critical to estimate the PD charge uncertainty.**

Keywords—partial discharge, IEC 60270, calibration, uncertainty, UHF.

I. Introduction

Partial discharge (PD) measurement is an accepted indicator of the electric insulation condition and is required for gas-insulated substations (GIS) in the standard IEC-62271 [1]. This standard refers to the IEC 60270 [2] for PD measurements, consisting of a device under test (DUT) measured with a coupling capacitor, where the PD pulse flows through the HV capacitor (C_1) and the coupling device (CD). Then the PD is filtered and measured in the measuring instrument (MI), as shown in Fig. 1. The calibration consists in finding a calibration constant by relating a known charge with the measured peak signal. The IEC method assumes that the calibrator is connected to the terminals where the PD happens, which is true for small objects that can be modeled as lumped elements. However, when the pulse wavelength is comparable with the device's length, the DUT behaves as a distributed element, shifting the calibrator's and the PD's electric position [3].

"This project 19ENG02 FutureEnergy has received funding from the EMPIR programme co-financed by the Participating States and from the European Union's Horizon 2020 research and innovation programme").

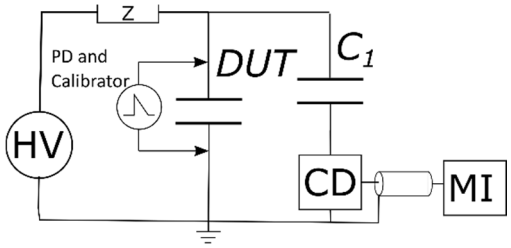

Fig. 1. IEC 60270 measuring circuit.

Onsite GIS installations are generally terminated to a cable or a transformer, making the energized conductor inaccessible for the calibrator and the coupling capacitor (CC) connection. Additionally, an online monitoring HV CC installation is expensive. Therefore, the IEC 60270 proposes the ultra-high frequency sensor (UHF) as an alternative way to calibrate and measure PD, as shown in Fig. 2. The calibration is done with a step voltage connected to the UHF sensor, generating a current pulse at the sensor's coupling capacitance. In the same way, the pulse is measured with the UHF sensors and GIS mutual capacitance.

The UHF sensor is a practical way to implement the IEC 60270 for no accessible HV conductors. However, the low coupling capacitance introduces uncertainty to the calibration procedure. This paper analyses the sources of uncertainties using the standard method with an external coupling capacitor and the UHF sensor. First, the GIS's calibrator location and pulse width are simulated as transmission lines (TL) and lumped elements. Then, the noise influence in UHF sensors is analysed for different filters and output loads. Finally, the error of the IEC method is measured in a full-scale GIS.

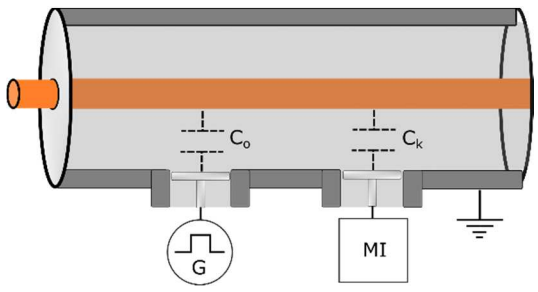

Fig. 2. IEC 60270 recommendation for PD in GIS.

II. IEC 60270 SIMULATION ON GIS

A. Calibration location uncertainty

One source of uncertainty is the calibrator location relative to the PD source, which depends on the GIS length. The GIS behaves as a transmission line in the transverse electromagnetic mode, distorting the PD signal in every discontinuity. Because of the IEC 60270 low-frequency range, the GIS can be modeled as a lossless transmission line [4], [5]. A time domain simulation was performed in LTspice, assuming the worst case, where the calibrator is at the opposite position of the PD source. Fig. 3 shows the electric representation of a simplified GIS. A pulse source is matched to the GIS and terminated with the coupling capacitor and the coupling device. Connected to the coupling device, a second-order bandpass filter was simulated, where the peak voltage was taken.

Fig. 4 shows the peak voltage ratio for different GIS lengths and two IEC bandwidths (BW): 30-130 kHz and 100-500 kHz. Using the lowest filter frequency in a 50 meters GIS, the error already approaches 10%, which is the limit acceptable for the IEC. The error exceeds the standard's limit when the highest bandwidth filter is used in a 10 m GIS. The lowest bandpass filter offers the lowest uncertainty when considering the GIS length. However, the filter selection must consider the noise sources in the GIS, where low-frequency noises are more critical. Additionally, low-frequency and narrow-band filters overlap subsequent PD pulses, increasing the charge error.

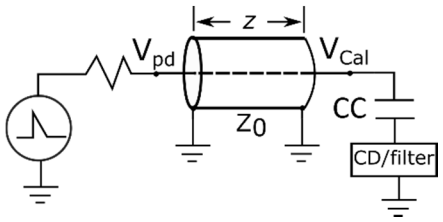

Fig. 3. GIS and coupling capacitor represented as a transmission line and a lumped capacitor.

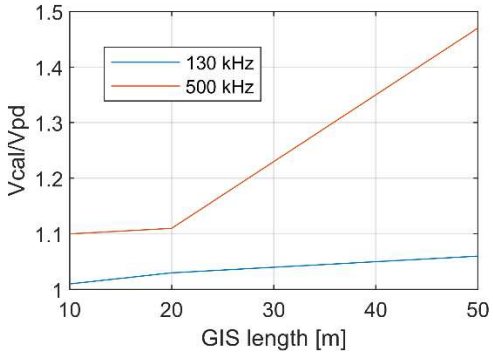

Fig. 4. Calibrator and PD pulse peak ratio for different GIS lengths.

B. Calibrator pulse width uncertainty

An SF_6 PD pulse lasts below one nanosecond [6], which is hundreds of times faster than a commercial calibrator. This difference in time may affect the calibration when the sensor's frequency response is not flat, which is the UHF sensor's case. A capacitor coupler's transfer function can be represented using (1) [7]. Since the UHF sensor has a small LV capacitance (C_2), the cutoff frequency ($\omega_0=1/C_2R$) happens at a frequency above the calibrator's bandwidth, affecting the calibration constant. An alternative way to decrease the ω_0 is to increase the sensor's load (R).

$$V_o(\omega) \approx \frac{I_{pd}(\omega)\, j\omega R C_1 Z_0}{-\omega^2 L C_2 + j\omega C_2 R + 1} \tag{1}$$

The GIS with external CC and UHF sensors were simulated in LTspice as transmission lines and lumped elements. The model recreates the TUDelft 1-phase-420kV GIS, composed of different discontinuities. The straight lines, T-sections, spacers, circuit breaker (CB), and disconnector are modeled as a time delay and characteristic impedance (Z_0) [8][9][10]. The straight-lines and T-sections characteristic impedance was taken as 75 Ω, and the rest as 50 Ω. The time delays for the spacers were 2 ns, and the rest are shown in Fig. 5. The overhead line bushing and the IEC external capacitors were modeled as lumped elements in series (L=10 µH, C_1=200 pF, C_2=90 µF). Finally, the calibration and PD pulse were simulated as a 200 ns and 1 ns step voltage in series with a 10 pF capacitor. Table 1 shows each measuring system cutoff frequency and peak signal error between the calibrator and PD pulse.

The IEC 60270 requires the measuring system BW to be below the calibrator's cutoff frequency, which was the case for the external CC but not for the 50Ω-UHF sensor. Fig. 6 shows, for each sensor's output, a simulated PD and calibrator signal as a 1 ns and 100 ns Gaussian pulse, respectively. The 50 Ω-UHF is the most affected due to its high-frequency response.

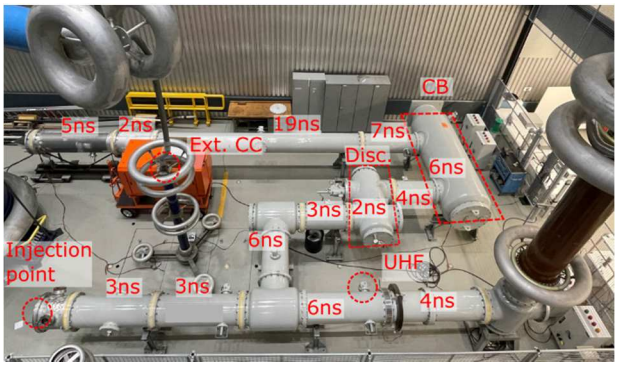

Fig. 5. TUDelft GIS with each discontinuity's time delay.

TABLE I. SENSOR'S CUTOFF FREQUENCIES AND ERROR BETWEEN CALIBRATOR AND PD PULSE.

	External CC	**50Ω-UHF**	**10kΩ-UHF**
f_0	100 kHz	159 MHz	796 kHz
Cal./PD	1%	13 %	4%

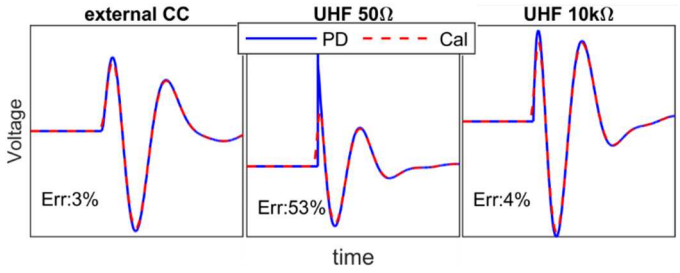

Fig. 6. Simulated PD and a calibrator waveshape comparison between an external CC, 50Ω-UHF, and 10kΩ-UHF. The calibrator's peak error is indicated in percentage.

C. Noise uncertainty

The UHF sensor's gain is increased with a larger load resistor, but the signal-to-noise ratio is also affected. The measured white noise at the sensor's output depends on the load resistor and the UHF sensor's LV capacitance, as shown in Fig. 7, where the noise source (V_n) is shown in (2), and the output noise (V_{NO}) in (3). When the IEC filter (H) is included, the RMS noise is shown in (4). The thermal noise density increases by the square root of the resistance; however, the sensor's output noise is filtered at $\omega=1/CR$, reducing the output noise.

$$V_n = \sqrt{4kTRf_{BW}} \tag{2}$$

$$V_{NO}(\omega) = V_n * \frac{1}{1 + j\omega R(C_2 + C_1)} \tag{3}$$

$$V_{rms_{NO}} \approx \sqrt{\int_0^{\infty} V_{NO}(\omega)^2 \left| H(\omega)^2 \right| d\omega} \tag{4}$$

The IEC charge is calculated using the output voltage peak, so the signal-peak-to-noise ratio (PSNR) is calculated for different filters. Fig. 8 shows the PSNR as a function of the load resistance with GIS's 5 pC permissible PD charge [11]. In the low-load region, the sensor's gain increases by the square root of the load; then, the gain settles down at the sensor's cutoff frequency. In the high-load region, the PSNR increases again with the load: the noise cutoff frequency becomes lower than the IEC filter's BW. Further research is planned to include the amplifier's noise. The filter selection must consider the higher PSNR but also the GIS length.

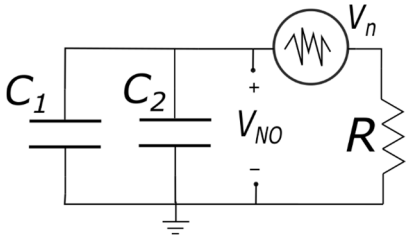

Fig. 7. Electric circuit representation of the noise.

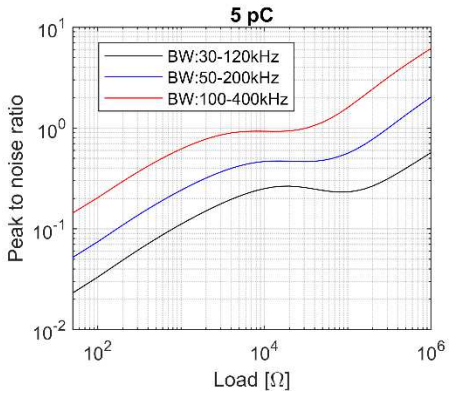

Fig. 8. PSNR as a function of the load/ and for different IEC filters' BWs.

III. Test Setup

The IEC 60270 with the external CC and the UHF were tested in parallel and compared with a high-frequency current transformer (HFCT) in the GIS shown in Fig. 5 and the setup in Fig. 9, using a 4 bar SF_6 jumping particle PD test cell. The external coupling capacitor consisted of a 200 pF HV capacitor connected to the bushing and a Haefely AKV 568 coupling device connected to a Haefely Type 561 instrument. The UHF sensor, shown in Fig. 10, has a 0.3 pF HV capacitance and a 17 pF LV capacitance. When the UHF sensor is not matched with 50 Ω, the capacitance of the coaxial cable connected from the sensor to the amplifier must be considered. The amplifier used for the UHF sensor was an AD8000, with an external input resistance of 10 kΩ, which was the maximum input resistance the amplifier could handle. The external CC and the UHF sensor were filtered with a 50-200 kHz second-order filter. The measurements were validated with an HFCT coupled to the test cell's ground electrode.

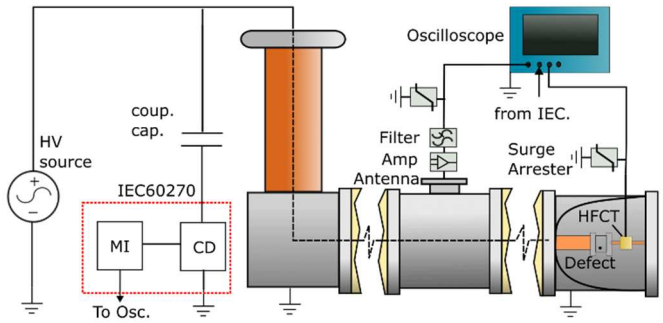

Fig. 9. Full-scale GIS test setup.

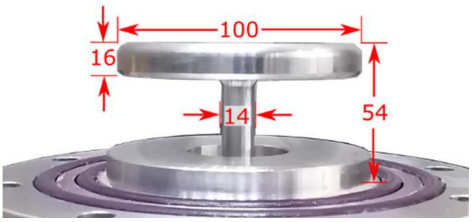

Fig. 10. UHF sensor used for the PD tests.

IV. Results and Discussion

shows the calibration results using an "Onsite high voltage Cal 141" with a 5 ns rise time and a 55 ns decay time and an "LDC-5/UHF" calibrator with a 1 ns rise time and 4.5 ns decay time. The external CC does not suffer any deviation when using different calibrators, unlike the UHF sensor, where a 5% difference was observed, giving a similar result to the simulation. Overall, the deviation is within the standard's 10% error tolerance. The 50Ω-UHF was not tested due to its low PSNR. Additionally, the external CC correlates with the HFCT, giving an average error of 4% and a standard deviation of 5%. The charge of HFCT was estimated using the current integral method [12]. The IEC output was rectified to estimate the PD charge with the absolute max pulse peak.

Fig. 11 compares the 10 kΩ-UHF sensor and the external CC, having a mean error of -2% and a standard deviation of 14%. The uncertainty of the UHF sensor is attributed to the white noise, explaining the low mean error and higher standard deviation. Fig. 12 shows the waveshape of both measurements, where the UHF PD signal is affected by noise. Further research is needed to improve the PSNR using an amplifier loaded with higher input impedance and a UHF sensor design adapted for IEC 60270 frequency.

TABLE II. Calibrators' peak values at different locations and sensors.

	External CC	10kΩ-UHF
Cal141/LCD5	0%	5%

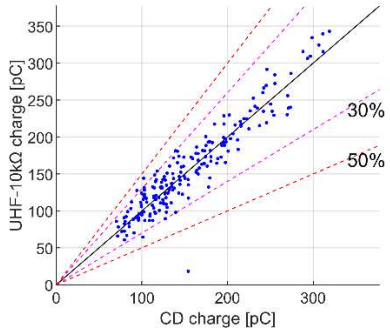

Fig. 11. PD charge values between the IEC ext. CC and 10 kΩ-UHF (dashed lines represent 30% and 50% error limits, respectively).

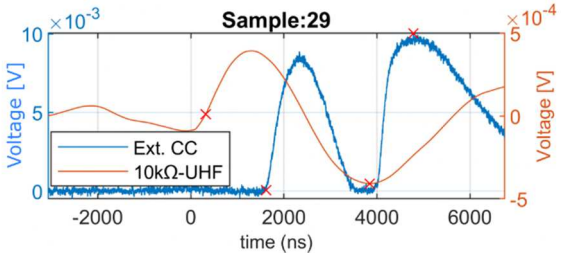

Fig. 12. Measured PD pulse with external CC and UHF sensor. With the pulse starting point and peak values marked with a red cross.

V. Conclusions

PD charge magnitude is valuable for assessing the condition of electric devices and normalizing different PD sensors. The IEC 60270 has been proven to be an excellent tool for electrically small devices; however, as the equipment grows in size, the uncertainty of the measurement increases. As the IEC method is not suitable for onsite and online tests, an alternative method is to use UHF sensors as the calibrator and coupling capacitor. This paper analyses different uncertainty sources and proposes the most convenient filters depending on the situation. The external coupling capacitor IEC test showed satisfying results for a 25 m long GIS. Also, a good correlation using a 10 kΩ-UHF sensor was found. Further research is needed to improve the UHF sensor's method and analyse its behaviour with more noise sources.

References

[1] INTERNATIONAL, ELECTROTECHNICAL, and COMMISSION, IEC 62271: High-voltage switchgear and controlgear – Part 203: AC gas-insulated metal-enclosed switchgear for rated voltages above 52 kV, vol. 3. 2022.

[2] B. Standard, "IEC 60270 : partial discharge measurements," Br. Stand., 2001, [Online]. Available: http://cds.cern.ch/record/840339

[3] A. Cavallini, G. C. Montanari, and M. Tozzi, "PD apparent charge estimation and calibration: A critical review," IEEE Trans. Dielectr. Electr. Insul., vol. 17, no. 1, pp. 198–205, 2010, doi: 10.1109/TDEI.2010.5412018.

[4] S. Meijer, Partial Discharge Diagnosis of High-Voltage Gas-Insulated Systems. Delft, 2001.

[5] R. Kurrer, Teilentladungsmessung im Gigaherts-Frequencbereich an SF6-isolierten Schaltanlagen. Stuttgart, 1997.

[6] A. J. Reid, M. D. Judd, B. G. Stewart, and R. A. Fouracre, "Partial discharge current pulses in SF6 and the effect of superposition of their radiometric measurement," J. Phys. D. Appl. Phys., vol. 39, no. 19, pp. 4167–4177, 2006, doi: 10.1088/0022-3727/39/19/008.

[7] C. Mier, A. Rodrigo Mor, L. Castro, and P. Vaessen, "Magnetic and electric antennas calibration for partial discharge charge estimation in gas-insulated substations," Int. J. Electr. Power Energy Syst., vol. 141, no. January, p. 108226, 2022, doi: 10.1016/j.ijepes.2022.108226.

[8] M. Hikita, S. Ohtsuka, S. Okabe, J. Wada, T. Hoshino, and S. Maruyama, "Influence of Insulating Spacer Type on Propagation Properties of PD-induced Electromagnetic Wave in GIS," IEEE Trans. Dielectr. Electr. Insul., vol. 17, no. 6, pp. 1731–1737, 2010, doi: 10.1109/TDEI.2010.5658223.

[9] H. Imagawa et al., "PD signal propagation characteristics in GIS and its location system by frequency components comparison," IEEE Trans. Power Deliv., vol. 16, no. 4, pp. 564–570, 2001, doi: 10.1109/61.956738.

[10] W. Gao, D. Ding, D. Zhao, and W. Liu, "Propagation properties of high-frequency electromagnetic wave through typical in-field GIS structures," IEEE Trans. Power Deliv., vol. 29, no. 6, pp. 2476–2484, 2014, doi: 10.1109/TPWRD.2014.2356500.

[11] C. W. 33/23.12, "Insulation Co-ordination of GIS: return of experience, on site tests and diagnostic techniques," 1998.

[12] A. R. Mor, P. H. F. Morshuis, and J. J. Smit, "Comparison of charge estimation methods in partial discharge cable measurements," IEEE Trans. Dielectr. Electr. Insul., vol. 22, no. 2, pp. 657–664, 2015, doi: 10.1109/TDEI.2015.7076760.